Biased Ising Model Using Two Coupled Kerr Parametric Oscillators with External Force

Pablo Álvarez,[1] Davide Pittilini,[1] Filippo Miserocchi,[1] Sathyanarayanan Raamamurthy,[1] Gabriel Margiani,[1] Orjan Ameye,[2] Javier del Pino,[3] Oded Zilberberg,[2] and Alexander Eichler[1,4]

[1]*Laboratory for Solid State Physics, ETH Zürich, CH-8093 Zürich, Switzerland*
[2]*Department of Physics, University of Konstanz, D-78457 Konstanz, Germany*
[3]*Institute for Theoretical Physics, ETH Zürich, CH-8093 Zürich, Switzerland*
[4]*Quantum Center, ETH Zürich, CH-8093 Zürich, Switzerland*

(Received 19 July 2023; accepted 9 April 2024; published 17 May 2024)

Networks of coupled Kerr parametric oscillators (KPOs) are a leading physical platform for analog solving of complex optimization problems. These systems are colloquially known as "Ising machines." We experimentally and theoretically study such a network under the influence of an external force. The force breaks the collective phase-parity symmetry of the system and competes with the intrinsic coupling in ordering the network configuration, similar to how a magnetic field biases an interacting spin ensemble. Specifically, we demonstrate how the force can be used to control the system, and highlight the crucial role of the phase and symmetry of the force. Our Letter thereby provides a method to create Ising machines with arbitrary bias, extending even to exotic cases that are impossible to engineer in real spin systems.

DOI: 10.1103/PhysRevLett.132.207401

The Kerr parametric oscillator (KPO) is a nonlinear resonator with a time-dependent harmonic potential term [1–16]. In a certain range of parameters, this potential modulation renders the zero-amplitude solution unstable. There, the system undergoes a spontaneous period-doubling Z_2 symmetry-breaking phase transition and assumes a large-amplitude oscillation at a so-called phase state. Importantly, a KPO features two such phase states with equal amplitude but phases separated by π, shown as black dots in Fig. 1(a).

The KPO is at the focus of much research work because its two phase states are analogous to the two polarization states of an Ising spin, "up" and "down." Consequently, it was proposed that networks of KPOs can be used to find the ground state of Ising Hamiltonians, that is, the energetically preferred configuration of a spin network [18]. Such resonator-based Ising solvers [14,19–22] are of high interest because the corresponding calculations are NP-hard (where NP stands for nondeterministic polynomial time) to tackle with conventional computers [23], and yet they map to many other key optimization problems, such as the travelling salesman problem [24], the MAX-CUT problem [25,26], and the number partitioning problem [27]. In Fig. 1(b), we sketch a network of two spins, where each spin takes the form of a double-well potential whose wells corresponds the two levels ("spin up" or "spin down").

Previous experimental and theoretical studies of KPO-based Ising simulators with bilinear coupling considered the case of unbiased Ising Hamiltonians, where the solutions are only defined up to a global sign [17,20,27–33]. For example, the state "down-up" shown in Fig. 1(b) can be identically replaced by "up-down," as the individual spin levels are

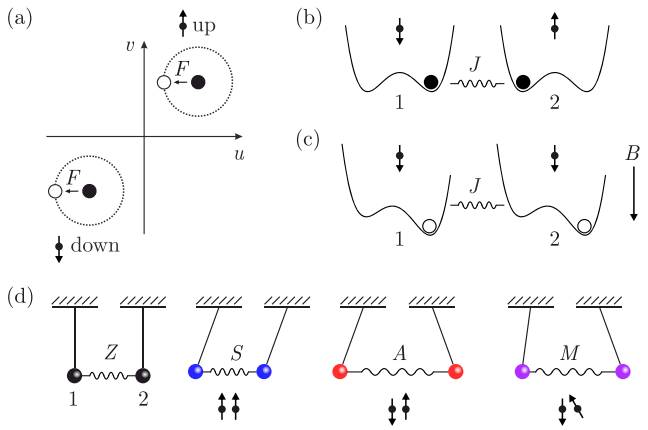

FIG. 1. KPOs as Ising spin analogues. (a) KPO phase states in a rotating phase space spanned by the quadratures u and v, where $x = u\cos(2\pi f_d t) - v\sin(2\pi f_d t)$, with f_d the driving frequency. Stationary solutions in the absence of an external force are shown as black dots and are labeled "up" and "down" to indicate a formal similarity to the two states of an Ising spin, marked by arrow symbols. Solutions in the presence of an external force F are shown as white dots as a function of the force phase θ (dotted circle). (b) Representation of a two-spin network as coupled double wells in the absence of a bias field. The levels of each double well (1,2) are energetically degenerate. The spin-spin coupling is indicated by J and leads to an antisymmetric state in this example. (c) In the presence of a bias field B, the degeneracy is broken and each spin has a preferred polarization. This preference can overcome the solution favored by the coupling J. (d) Coupled resonators are often described in a normal-mode basis as illustrated by two coupled pendula. For two KPOs, the relevant nonlinear stationary states we will refer to in this Letter include states with zero amplitude (Z), symmetric (S) and antisymmetric (A) oscillation, as well as mixed-symmetry (M) solutions. The latter denote oscillations that are neither fully symmetric nor antisymmetric [17].

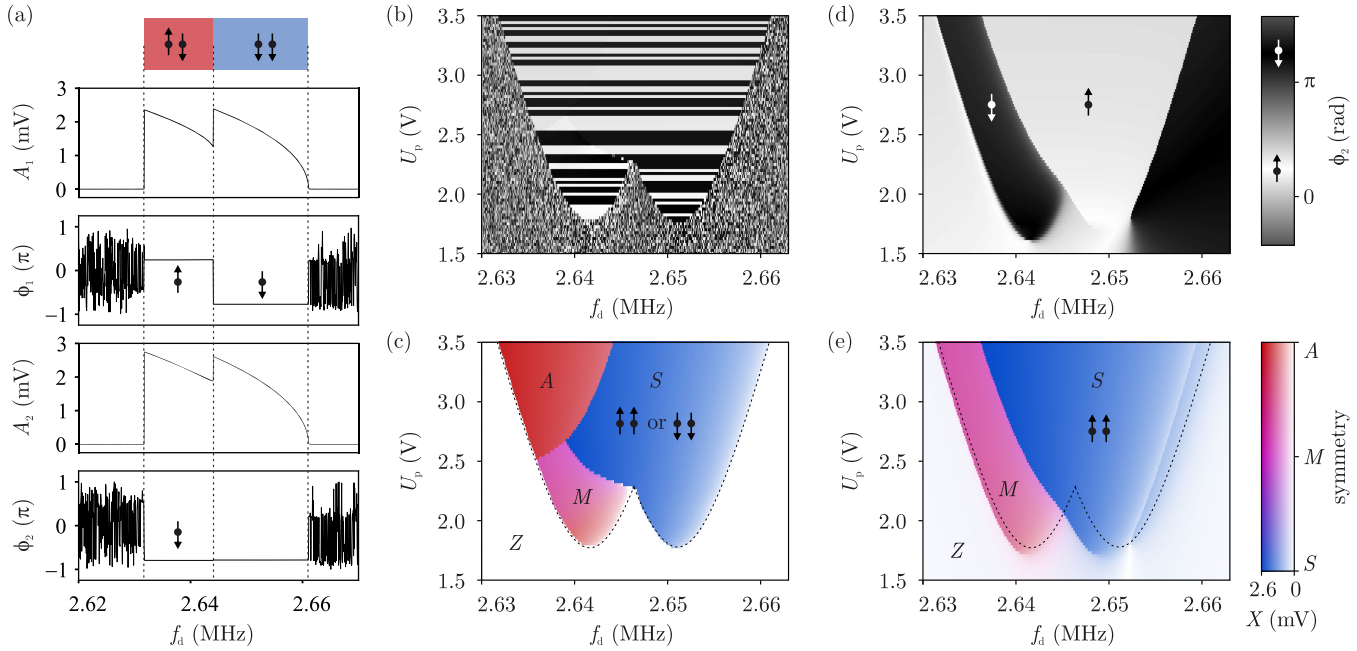

FIG. 2. (a) Measured amplitudes A_i and phase responses ϕ_i of the two resonators when driven by a parametric pump tone with $U_p = 3.5$ V. The arrow symbols represent the Ising spin analogy, and the colors indicate the relative phase configuration. (b) Measured phase ϕ_2 as a function of f_d and U_p for $U_d = 0$, where $U_d \propto F$ is a driving voltage [38]. (c) Measured amplitude and phase configuration of the two resonators for $U_d = 0$. Dashed lines are theory predictions for the outline of the characteristic double tongue. (d) Same as (b) with a force strength $U_d = 10$ mV at a phase $\theta = 55°$. This value of θ was found to strongly favor the symmetric state with $\phi_{1,2} \approx 45° = 0.78$ rad. (e) Measured amplitude and phase configuration of the two resonators for $U_d = 10$ mV and $\theta = 55°$. Dashed lines mark the outlines calculated for (c) to highlight the shifted boundaries.

degenerate. Many Ising problems, however, require breaking of this degeneracy; the archetypal case being a magnetic field applied to a spin ensemble. In Fig. 1(c), a magnetic field B biases the potential to compete with the spin-spin coupling J. A strong field can overcome the coupling-induced ordering and dramatically change the configuration that emerges as the optimal solution of the spin system. These solutions can be characterized in terms of the normal modes of the oscillator network in the linear regime, see Fig. 1(d) [17,33,34]. The external field functionality was recently included in optical parametric systems with dissipative coupling [35], which constitute an alternative route towards Ising simulators [36,37].

In this Letter, we demonstrate experimentally how the functionality of an external B field can be introduced in a classical KPO network. By applying an external force F to each resonator, we can displace the network's solutions in their phase space, as indicated in Fig. 1(a). Our experiment features two coupled KPOs, but the concepts we present are easily extended to larger networks. We provide a general framework to understand the role of the external force term for coupled KPOs and resonator-based Ising solvers. Importantly, while this forcing can emulate the effect of a simple bias field, we show that its consequences are much richer due to the freedom of selecting the driving amplitude and phase for each resonator individually. Our Letter will therefore not only provide a practical guide for applications, but also motivate further fundamental research on Ising networks with inhomogeneous magnetic fields, including quantum implementations [12,20,28,30].

Our experiment consists of two electrical resonators that feature a nonlinear capacitance [10]. The system can be described by the coupled differential equations

$$\ddot{x}_i + \omega_0^2[1 - \lambda\cos(4\pi f_d t)]x_i + \beta x_i^3 + \Gamma\dot{x}_i - Jx_j = F_i(t), \tag{1}$$

where the displacement x_i is the measured voltage signal of resonator i [10,17] as a function of time t. The angular resonance frequency $\omega_0/2\pi = f_0 = 2.646$ MHz, the damping rate $\Gamma = (\omega_0/Q) = 73$ kHz, the parametric modulation depth λ, and the nonlinearity β are approximately equal for both resonators, see section S1 in the Supplemental Material [38]. Finally, J quantifies the coupling between the resonators ($j \neq i$), and the $F_i(t)$ are external forces applied to the resonators individually. We experimentally implement the forces with driving voltages $U_d \propto F$ [38]. In the following, we will study the competition between these two effects (J versus F_i) in ordering the phases of the two KPOs. All phases are measured relative to the same reference clock unless

otherwise stated. The phases of the parametric pump terms are set to zero and are therefore not shown in Eq. (1).

In Fig. 2(a), we demonstrate a frequency sweep by slowly increasing f_d at a constant pump amplitude $U_p \propto \lambda$ [38] with $F_i = 0$. We use lock-in amplifiers (Zurich Instruments MFLI) to measure the amplitudes $A_i = (u_i^2 + v_i^2)^{1/2}$ and phases $\phi_i = \arctan(v_i/u_i)$ of the two resonators, where $x = u\cos(2\pi f_d t) - v\sin(2\pi f_d t)$. We observe that both resonators jump from zero to a finite amplitude around 2.63 MHz. The phase of the two resonators assumes a well-defined value after the jump, with $\phi_1 - \phi_2 = \pi$. In our spin analogy, this corresponds to an antisymmetric ordering (up-down). Around 2.645 MHz, the amplitudes jump again, accompanied by a π shift of ϕ_1. The resulting state is analogous to a symmetric spin state ("down-down"). Roughly at 2.66 MHz, the amplitudes drop to zero and the phases become random again.

We repeat frequency sweeps at different values of U_p. In Fig. 2(b), the measured ϕ_2 as a function of f_d and U_p is plotted. We clearly see that in each sweep, the phase assumes a well-defined value in a certain frequency range described by two overlapping, rounded triangles often called "Arnold tongues" [17,40]. Importantly, the phase randomly assumes one of two values separated by π in each sweep. This randomness is a consequence of the symmetry illustrated in Fig. 1(b), and the resulting spontaneous time-translation symmetry breaking at each jump from zero to finite amplitude. It is a fundamental feature of a KPO, and of networks thereof, in the absence of an external force.

To map the different symmetry phases of the system, we employ the symmetric and antisymmetric quadratures $v_S = (1/\sqrt{2})(v_1 + v_2)$ and $v_A = (1/\sqrt{2})(v_1 - v_2)$. Note that $u_{S,A}$ can be defined analogously and yield qualitatively similar results. In Fig. 2(c), we represent the total amplitude $X = (v_S^2 + v_A^2)^{1/2}$ as a brightness contrast, while the relative phase of the two resonators is shown in color code. As in a previous work [17], we observe S, A, and M phases inside the overlapping Arnold tongues. The center frequencies and phase symmetries of the two Arnold tongues are inherited from the normal modes of the system in the linear regime. The precise shapes of these zones are understood to originate from an interplay of the nonlinearity β and the coupling J, and can be reproduced precisely with numerical simulations and with an analytical solver [38,41].

In the next step, we additionally apply an external force to each resonator. For simplicity, we select $F_i(t) = F\cos(2\pi f_d t + \theta)$ for both resonators, with θ a global phase. Note that F_i (and therefore U_i) are applied at exactly half the frequency of the parametric pump. In Fig. 2(d), we see a striking change in the measured ϕ_2 compared to Fig. 2(b): the phase now exhibits a well-defined value over the entire parameter space, and the jump between solutions follows a deterministic pattern. The spontaneous time-translation symmetry breaking observed in Fig. 2(b) is entirely replaced by a force-induced bias, as sketched in Fig. 1(c). The force therefore allows us to control the "spin polarization" of the individual KPOs in each sweep.

When plotting the system states in Fig. 2(e), we find several important differences to the unbiased example in Fig. 2(c). First, the outlines of the Arnold tongues are shifted by the force. This effect arises due to changes in the stability conditions of the parametric oscillators, which was previously studied for the case of a single KPO [1,5,10,42–44]. The most prominent manifestation of this effect is a jump (of both phase and amplitude) at the right border of the S phase. This jump is caused by the termination of the selected symmetric phase state [38]. For a symmetric force, we mainly observe a shift of the S region. Second, the antisymmetric state labeled A is no longer visible, as it is not favored by the symmetric force. Numerical simulations indicate that the A state still appears at higher values of U_p, where the impact of the external force is reduced relative to the parametric pump. The symmetric state S therefore fills a greater portion of the diagram, in agreement with the intuition that a symmetric force $F_1 = F_2$ should favor this phase configuration. Third, the S state now only comprises an "up-up" component, instead of allowing both up-up and "down-down" as in Fig. 2(c). The force therefore fulfills the role of a potential bias, as anticipated.

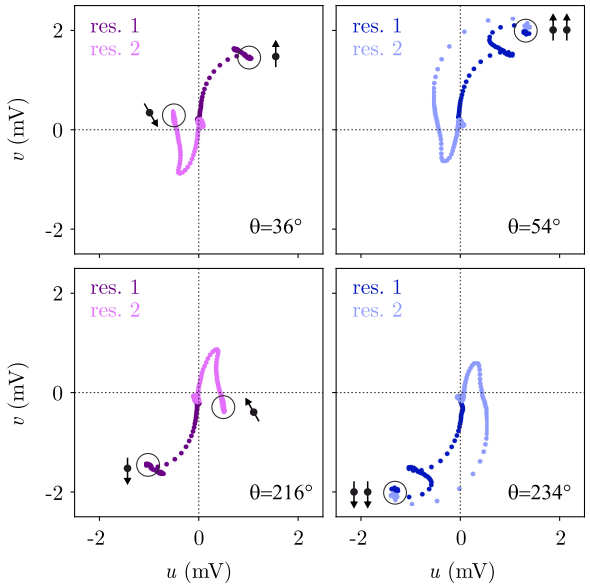

FIG. 3. Ringup experiments with different values of force phase θ. Both resonators are initialized in $u_i = 0$ and $v_i = 0$ (center of graphs). First, only an external force $U_d = 20$ mV with phase θ is applied to break the symmetry, bringing the resonators to an amplitude of ≈0.1 mV. Then the parametric pump $U_p = 3.15$ V is added and the resonators ring up to symmetric or mixed-symmetry solutions, as marked by white disks. Arrow symbols indicate the corresponding spin analogy. All experiments were performed at $f_d = 2.639$ MHz.

In Fig. 2, we employ frequency sweeps with a fixed force phase θ to study the solution space of our system. In many applications, however, it may be more useful to start from the equilibrium state of the unforced system ($u_i = 0$ and $v_i = 0$), and then directly access a particular solution through the correct choice of θ. We demonstrate this capability experimentally in Fig. 3, where the system rings up to four different symmetric and mixed-symmetry states, depending on the phase θ of the symmetric external force. In the spirit of the two-spin analogy that we employ throughout the paper, we label the final states with corresponding symbols. We find that small changes in θ can cause the system to attain an entirely different state. For instance, $\theta = 36°$ leads to a symmetric state while $\theta = 54°$ leads to a mixed-symmetry state. Rotating θ by 180° inverts the final state of both resonators, leaving the relative configuration intact (e.g., up-up becomes down-down).

The deterministic experiments we reported so far always reach the same stable solutions for the same initial conditions and driving parameters. This leads to a limited understanding of our system, which possesses several stable solutions for certain positions in the f_d-U_p diagram [38]. Stochastic sampling allows us to explore these different solutions, and to assess their dwell times in the long-time limit [33]. In Fig. 4(a), we show how the system jumps between different solutions when activated by white noise and in the absence of external forcing ($F_i = 0$). For most of the time, the system jumps between the two symmetric solutions, which are more stable than the antisymmetric solutions due to their higher amplitude. A high amplitude imposes a larger "momentum barrier" and makes the state more stable against jumps [33]. In a so-called symmetry space spanned by v_S and v_A, these dynamics result in the plot shown in Fig. 4(b). Here, symmetric and antisymmetric states appear at the corners of a diamond at $v_A = 0$ and $v_S = 0$, respectively (plots for the u_S and u_A look very similar). The edges of the diamond result from points measured during transitions between the states. As insets, we sketch the corresponding picture of two spins without an external field, allowing both symmetric and antisymmetric states (and fluctuations between them).

When applying an external force, we can change the relative weight (occupation probability) of these four states. In Figs. 4(c) and 4(d), we apply symmetric forces whose phase θ is tuned to favor either of the two symmetric states. As a consequence, we observe the system only in the corresponding symmetric state, and all jumps are

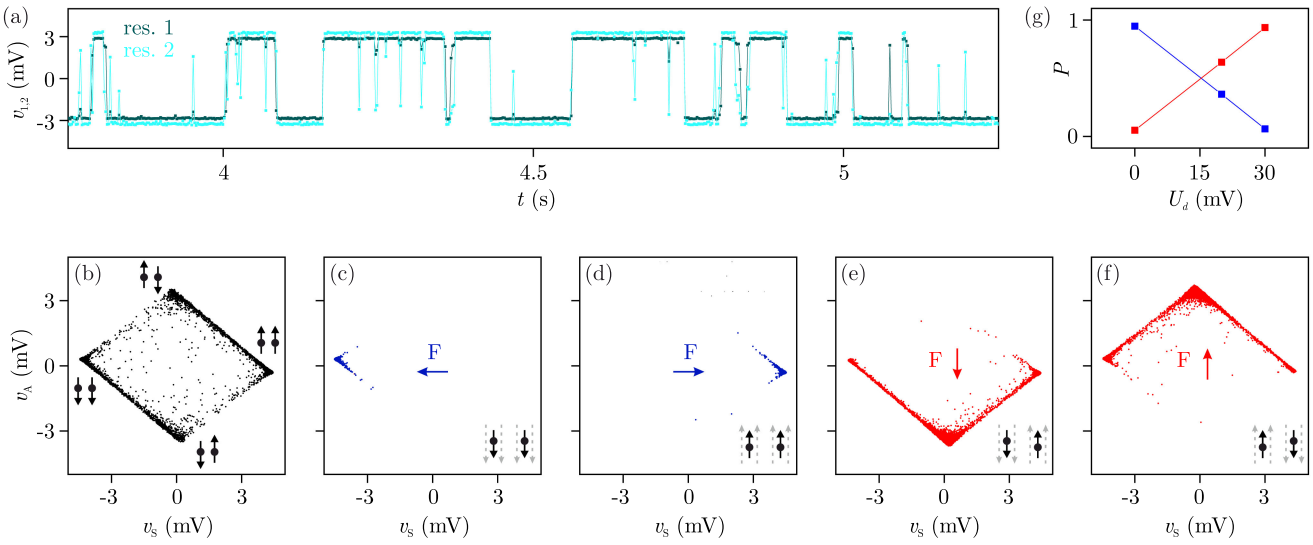

FIG. 4. Stochastic sampling of KPO network states. (a) Quadratures v_1 and v_2 measured as a function of time in the presence of force noise. The applied noise is white up to approximately 30 MHz and has a standard deviation of 350 mV. Separate noise generators were employed for the two KPOs and connected via additional inductive lines. Only the v_i are shown here for simplicity. $U_p = 3.5$ V, $U_d = 0$, lock-in demodulation rate $B = 500$ Hz, and $f_d = 2.586$ Hz (the resonance frequencies of both KPO shifted due to the additional inductive lines). (b) Representation of the time trace from (a) in a so-called symmetry space spanned by $v_S = (1/\sqrt{2})(v_1 + v_2)$ and $v_A = (1/\sqrt{2})(v_1 - v_2)$. The stable solutions of the system in the absence of noise are at the corners of the diamond. (c) A symmetric force of 30 mV with $\theta = 0$ (after subtracting a global phase offset of -46°) favors the negative symmetric state. (d) With $\theta = 180°$, the symmetric force favors the positive symmetric state. (e) An antisymmetric force with $\theta_1 = 0$ and $\theta_2 = 180°$ favors the negative antisymmetric state. (f) inverting both phases favors the positive antisymmetric state. A total of 60s of data was taken for each case. Insets show spin with grey dashed arrows for the local magnetic field direction. (g) Measured probability P of finding the system in the symmetric (blue) and antisymmetric (red) configuration as a function of antisymmetric driving voltage U_d. Points at 0 mV and 30 mV correspond to the data in (b) and (e),(f), respectively. For details see Ref. [38].

suppressed. The spin picture with external field below each graph shows how the spins are forced to align by the homogeneous external field.

In contrast to a real (nanoscale) spin ensemble, our system allows us to arbitrarily tune the amplitude and phase of the applied force (corresponding to the strength and direction of the external field) for each KPO individually. As a demonstration example, we show in Figs. 4(e) and 4(f) the results for an antisymmetric force $F_i(t) = F\cos(2\pi f_d t + \theta_i)$ with $\theta_2 = -\theta_1$. Here, we find that the system occupies almost exclusively the selected antisymmetric state. However, the suppression of the symmetric states is weaker than in the opposite case in Figs. 4(c) and 4(d). Again, this is due to the fact that the symmetric state is generally more stable than the antisymmetric state for $J/\beta > 0$ [33]. Even larger forces would be necessary to entirely overcome this intrinsic bias.

The statistical state distribution of coupled KPOs for weak coupling and $F = 0$ was studied previously [30,45]. Our experiment is in the limit of strong coupling and $F \neq 0$, for which no analytical solution exists. However, we experimentally study the transition between the regime dominated by J to an ordering imposed by F in Fig. 4(g). More details and additional simulations can be found in [38].

In our experiments and in the theory analysis, we find that the external force can bias our system of coupled KPOs. In the simplest case, this bias is analogous to an external magnetic field acting on an ensemble of coupled spins. The tunable phase θ of the external force assumes the role of the magnetic field angle, which can be different for each KPO, cf. Figs. 3 and 4. This freedom in selecting the phases will be crucial in future experiments that go beyond conventional spin systems, as it allows access to unexplored, exotic networks that have no counterpart in solid state physics. Such novel networks include, for instance, the Ising chain in the presence of a tunable local impurity [46], the random-field Ising model [47–50] and corresponding avalanche models [51–54], and the magnetic Bose polaron [55]. We believe that controlled experimental realizations of these elusive phenomena will spur new developments in theory in many directions. At the same time, our Letter demonstrates new strategies to control Ising machines, and to program such systems to solve complex optimization tasks [23–27].

We acknowledge funding from the Deutsche Forschungsgemeinschaft (DFG) via Project No. 449653034 and through SFB1432, as well as the Swiss National Science Foundation (SNSF) through the Sinergia Grant No. CRSII5_206008/1.

[1] D Ryvkine and M I Dykman, Resonant symmetry lifting in a parametrically modulated oscillator, Phys. Rev. E **74**, 061118 (2006).

[2] I. Mahboob and H. Yamaguchi, Bit storage and bit flip operations in an electromechanical oscillator, Nat. Nanotechnol. **3**, 275 (2008).

[3] C. M. Wilson, T. Duty, M. Sandberg, F. Persson, V. Shumeiko, and P. Delsing, Photon generation in an electromagnetic cavity with a time-dependent boundary, Phys. Rev. Lett. **105**, 233907 (2010).

[4] Alexander Eichler, Julien Chaste, Joel Moser, and Adrian Bachtold, Parametric amplification and self-oscillation in a nanotube mechanical resonator, Nano Lett. **11**, 2699 (2011).

[5] Alexander Eichler, Toni L. Heugel, Anina Leuch, Christian L. Degen, Ramasubramanian Chitra, and Oded Zilberberg, A parametric symmetry breaking transducer, Appl. Phys. Lett. **112**, 233105 (2018).

[6] Jan Gieseler, Bradley Deutsch, Romain Quidant, and Lukas Novotny, Subkelvin parametric feedback cooling of a laser-trapped nanoparticle, Phys. Rev. Lett. **109**, 103603 (2012).

[7] Z. R. Lin, K. Inomata, K. Koshino, W. D. Oliver, Y. Nakamura, J. S. Tsai, and T. Yamamoto, Josephson parametric phase-locked oscillator and its application to dispersive readout of superconducting qubits, Nat. Commun. **5**, 4480 (2014).

[8] S. Puri, S. Boutin, and A. Blais, Engineering the quantum states of light in a Kerr-nonlinear resonator by two-photon driving, npj Quantum Inf. **3**, 18 (2017).

[9] Alexander Eichler, Toni L. Heugel, Anina Leuch, Christian L. Degen, R. Chitra, and Oded Zilberberg, A parametric symmetry breaking transducer, Appl. Phys. Lett. **112**, 233105 (2018).

[10] Z. Nosan, P. Märki, N. Hauff, C. Knaut, and A. Eichler, Gate-controlled phase switching in a parametron, Phys. Rev. E **99**, 062205 (2019).

[11] Martin Frimmer, Toni L. Heugel, Ziga Nosan, Felix Tebbenjohanns, David Hälg, Abdulkadir Akin, Christian L. Degen, Lukas Novotny, R. Chitra, Oded Zilberberg, and Alexander Eichler, Rapid flipping of parametric phase states, Phys. Rev. Lett. **123**, 254102 (2019).

[12] Alexander Grimm, Nicholas E. Frattini, Shruti Puri, Shantanu O. Mundhada, Steven Touzard, Mazyar Mirrahimi, Steven M. Girvin, Shyam Shankar, and Michel H. Devoret, Stabilization and operation of a Kerr-cat qubit, Nature (London) **584**, 205 (2019).

[13] Zhaoyou Wang, Marek Pechal, E. A. Wollack, Patricio Arrangoiz-Arriola, Maodong Gao, N. R. Lee, and A. H. Safavi-Naeini, Quantum dynamics of a few-photon parametric oscillator, Phys. Rev. X **9**, 021049 (2019).

[14] Shruti Puri, Alexander Grimm, Philippe Campagne-Ibarcq, Alec Eickbusch, Kyungjoo Noh, Gabrielle Roberts, Liang Jiang, Mazyar Mirrahimi, M. H. Devoret, and S. M. Girvin, Stabilized cat in a driven nonlinear cavity: A fault-tolerant error syndrome detector, Phys. Rev. X **9**, 041009 (2019).

[15] James M. L. Miller, Dongsuk D. Shin, Hyun-Keun Kwon, Steven W. Shaw, and Thomas W. Kenny, Phase control of self-excited parametric resonators, Phys. Rev. Appl. **12**, 044053 (2019).

[16] T. Yamaji, S. Kagami, A. Yamaguchi, T. Satoh, K. Koshino, H. Goto, Z. R. Lin, Y. Nakamura, and T. Yamamoto, Spectroscopic observation of the crossover from a classical duffing oscillator to a Kerr parametric oscillator, Phys. Rev. A **105**, 023519 (2022).

[17] Toni L. Heugel, Oded Zilberberg, Christian Marty, R. Chitra, and Alexander Eichler, Ising machines with strong bilinear coupling, Phys. Rev. Res. **4**, 013149 (2022).
[18] Ernst Ising, Beitrag zur theorie des ferromagnetismus, Z. Phys. **31**, 253 (1925).
[19] Imran Mahboob, Hajime Okamoto, and Hiroshi Yamaguchi, An electromechanical Ising Hamiltonian, Sci. Adv. **2**, e1600236 (2016).
[20] H. Goto, Bifurcation-based adiabatic quantum computation with a nonlinear oscillator network, Sci. Rep. **6**, 21686 (2016).
[21] Leon Bello, Marcello Calvanese Strinati, Emanuele G. Dalla Torre, and Avi Pe'er, Persistent coherent beating in coupled parametric oscillators, Phys. Rev. Lett. **123**, 083901 (2019).
[22] Yoshitomo Okawachi, Mengjie Yu, Jae K. Jang, Xingchen Ji, Yun Zhao, Bok Young Kim, Michal Lipson, and Alexander L. Gaeta, Demonstration of chip-based coupled degenerate optical parametric oscillators for realizing a nanophotonic spin-glass, Nat. Commun. **11**, 4119 (2020).
[23] Naeimeh Mohseni, Peter L McMahon, and Tim Byrnes, Ising machines as hardware solvers of combinatorial optimization problems, Nat. Rev. Phys. **4**, 363 (2022).
[24] Andrew Lucas, Ising formulations of many NP problems, Front. Phys. **2**, 5 (2014).
[25] Takahiro Inagaki, Yoshitaka Haribara, Koji Igarashi, Tomohiro Sonobe, Shuhei Tamate, Toshimori Honjo, Alireza Marandi, Peter L. McMahon, Takeshi Umeki, Koji Enbutsu, Osamu Tadanaga, Hirokazu Takenouchi, Kazuyuki Aihara, Ken-ichi Kawarabayashi, Kyo Inoue, Shoko Utsunomiya, and Hiroki Takesue, A coherent Ising machine for 2000-node optimization problems, Science **354**, 603 (2016).
[26] Hayato Goto, Kosuke Tatsumura, and Alexander R. Dixon, Combinatorial optimization by simulating adiabatic bifurcations in nonlinear Hamiltonian systems, Sci. Adv. **5**, eaav2372 (2019).
[27] Simon E. Nigg, Niels Lörch, and Rakesh P. Tiwari, Robust quantum optimizer with full connectivity, Sci. Adv. **3**, e1602273 (2017).
[28] Shruti Puri, Christian Kraglund Andersen, Arne L. Grimsmo, and Alexandre Blais, Quantum annealing with all-to-all connected nonlinear oscillators, Nat. Commun. **8**, 15785 (2017).
[29] H. Goto, Z. Lin, and Y. Nakamura, Boltzmann sampling from the Ising model using quantum heating of coupled nonlinear oscillators, Sci. Rep. **8**, 7154 (2018).
[30] M. I. Dykman, Christoph Bruder, Niels Lörch, and Yaxing Zhang, Interaction-induced time-symmetry breaking in driven quantum oscillators, Phys. Rev. B **98**, 195444 (2018).
[31] Riccardo Rota, Fabrizio Minganti, Cristiano Ciuti, and Vincenzo Savona, Quantum critical regime in a quadratically driven nonlinear photonic lattice, Phys. Rev. Lett. **122**, 110405 (2019).
[32] Marcello Calvanese Strinati, Leon Bello, Avi Pe'er, and Emanuele G. Dalla Torre, Theory of coupled parametric oscillators beyond coupled Ising spins, Phys. Rev. A **100**, 023835 (2019).
[33] Gabriel Margiani, Javier del Pino, Toni L. Heugel, Nicholas E. Bousse, Sebastián Guerrero, Thomas W. Kenny, Oded Zilberberg, Deividas Sabonis, and Alexander Eichler, Deterministic and stochastic sampling of two coupled Kerr parametric oscillators, Phys. Rev. Res. **5**, L012029 (2023).
[34] Toni L. Heugel, Matthias Oscity, Alexander Eichler, Oded Zilberberg, and R. Chitra, Classical many-body time crystals, Phys. Rev. Lett. **123**, 124301 (2019).
[35] Hiroki Takesue, Kensuke Inaba, Takahiro Inagaki, Takuya Ikuta, Yasuhiro Yamada, Toshimori Honjo, Takushi Kazama, Koji Enbutsu, Takeshi Umeki, and Ryoichi Kasahara, Simulating Ising spins in external magnetic fields with a network of degenerate optical parametric oscillators, Phys. Rev. Appl. **13**, 054059 (2020).
[36] T. Inagaki, K Inaba, R. Hamerly, K Inoue, Y Yamamoto, and H. Takesue, Large-scale Ising spin network based on degenerate optical parametric oscillators, Nat. Photonics **10**, 415 (2016).
[37] Igor Gershenzon, Geva Arwas, Sagie Gadasi, Chene Tradonsky, Asher Friesem, Oren Raz, and Nir Davidson, Exact mapping between a laser network loss rate and the classical XY Hamiltonian by laser loss control, Nanophotonics **9**, 4117 (2020).
[38] See Supplemental Material at http://link.aps.org/supplemental/10.1103/PhysRevLett.132.207401 for additional setup descriptions and more measurement data, which includes Ref. [39].
[39] Paul Breiding and Sascha Timme, *International Congress on Mathematical Software* (Springer, 2018), pp. 458–465.
[40] Alexander Eichler and Oded Zilberberg, *Classical and Quantum Parametric Phenomena* (Oxford University Press, New York, 2023).
[41] Jan Košata, Javier del Pino, Toni L. Heugel, and Oded Zilberberg, HarmonicBalance.jl: A Julia suite for nonlinear dynamics using harmonic balance, SciPost Phys. Codebases **6** (2022).
[42] Jeffrey F. Rhoads and Steven W. Shaw, The impact of nonlinearity on degenerate parametric amplifiers, Appl. Phys. Lett. **96**, 234101 (2010).
[43] Luca Papariello, Oded Zilberberg, Alexander Eichler, and R. Chitra, Ultrasensitive hysteretic force sensing with parametric nonlinear oscillators, Phys. Rev. E **94**, 022201 (2016).
[44] Anina Leuch, Luca Papariello, Oded Zilberberg, Christian L. Degen, R. Chitra, and Alexander Eichler, Parametric symmetry breaking in a nonlinear resonator, Phys. Rev. Lett. **117**, 214101 (2016).
[45] C Han, M Wang, B Zhang, MI Dykman, and HB Chan, Controlled asymmetric Ising model implemented with parametric micromechanical oscillators, arXiv:2309.04281.
[46] H. Falk, Ising chain with a spin impurity, Phys. Rev. **151**, 304 (1966).
[47] G. Grinstein, Ferromagnetic phase transitions in random fields: The breakdown of scaling laws, Phys. Rev. Lett. **37**, 944 (1976).
[48] D. P. Belanger and A. P. Young, The random field Ising model, J. Magn. Magn. Mater. **100**, 272 (1991).
[49] N. S. Bingham, S. Rooke, J. Park, A. Simon, W. Zhu, X. Zhang, J. Batley, J. D. Watts, C. Leighton, K. A. Dahmen, and P. Schiffer, Experimental realization of the

1d random field Ising model, Phys. Rev. Lett. **127**, 207203 (2021).

[50] Liheng Yao and Robert L. Jack, Thermal vestiges of avalanches in the driven random field Ising model, J. Stat. Mech. (2023) 023303.

[51] Olga Perković, Karin Dahmen, and James P. Sethna, Avalanches, barkhausen noise, and plain old criticality, Phys. Rev. Lett. **75**, 4528 (1995).

[52] Mi-Young Im, Peter Fischer, Dong-Hyun Kim, and Sung-Chul Shin, Direct observation of individual barkhausen avalanches in nucleation-mediated magnetization reversal processes, Appl. Phys. Lett. **95**, 182504 (2009).

[53] Stuart Field, Jeff Witt, Franco Nori, and Xinsheng Ling, Superconducting vortex avalanches, Phys. Rev. Lett. **74**, 1206 (1995).

[54] Yoav Lahini, Omer Gottesman, Ariel Amir, and Shmuel M. Rubinstein, Nonmonotonic aging and memory retention in disordered mechanical systems, Phys. Rev. Lett. **118**, 085501 (2017).

[55] S. I. Mistakidis, G. M. Koutentakis, F. Grusdt, P. Schmelcher, and H. R. Sadeghpour, Inducing spin-order with an impurity: Phase diagram of the magnetic bose polaron, New J. Phys. **24**, 083030 (2022).